

International Journal of Modern Physics A
 © World Scientific Publishing Company

EFFECTS OF MODEL PARAMETERS IN THERMODYNAMICS OF THE PNJL MODEL

FRIESEN A.V.

*Bogoliubov Laboratory of Theoretical Physics, Joint Institute for Nuclear Research, 141980
Dubna, Russia
avfriesen@theor.jinr.ru*

KALINOVSKY Yu.L.

*Laboratory of Information Technologies, Joint Institute for Nuclear Research, 141980 Dubna,
Russia
Higher Mathematics Department, University "Dubna", Dubna, Russia
kalinov@jinr.ru*

TONEEV V.D.

*Bogoliubov Laboratory of Theoretical Physics, Joint Institute for Nuclear Research, 141980
Dubna, Russia
toneev@theor.jinr.ru*

Received Day Month Year

Revised Day Month Year

The thermodynamic behavior of the two-flavor ($N_f = 2$) three-color ($N_c = 3$) Polyakov-loop-extended Nambu–Jona-Lasinio model at the finite chemical potential is investigated. New lattice gluon data for gluon thermodynamics are used defining the effective potential within polynomial and logarithmic forms of its approximation. We study the effects of using different sets of data and different forms of the potential on thermodynamic properties of hot and dense matter. It is found that the PNJL thermodynamics depends stronger on the form of the effective potential than on the used lattice data set. Particular attention is paid to the phase diagram in the (T, μ) plane.

Keywords: PNJL model; phase diagram

PACS numbers: 11.30.Rd, 12.20.Ds, 14.40.Be

1. Introduction

In the last years the Polyakov-loop-extended Nambu–Jona-Lasinio (PNJL) model^{1–6} was widely used in the study of thermodynamics and the phase diagram of hot and dense matter. Results of this research are expected to play an important role in our understanding of the evolution of the early universe and physics of heavy ion collisions at relativistic energies. This improved field theoretical model is fundamental for interpreting the lattice QCD data and extrapolating into regions not yet accessible for lattice simulations.

An attractive property of the PNJL model is the synthesis of the Polyakov loop dynamics with the Nambu–Jona-Lasinio model, combining the two principal nonperturbative features of low-energy QCD: confinement and spontaneous chiral symmetry breaking. A particular feature of this model is that one can uniquely determine the coupling between the chiral condensate, which is an order parameter of the chiral phase transition when $m_q \rightarrow 0$, and the Polyakov loop, which is the order parameter for the deconfinement phase transition in the limit $m_q \rightarrow \infty$. The model is remarkably successful in reproducing lattice data on the QCD thermodynamics^{3,7–19}.

However, the choice of the parameter set as well as regularization of integrals, as noted by several authors, is a nontrivial question. As it is well known, the order of the phase transition in the (T, μ) plane is sensitive to the parameter choice. It was already noted^{4,20} that one can choose different sets of parameters which allow for a first order phase transition, giving a reasonable fit to physics observables in the vacuum but predicting different physical scenarios at finite temperature T and chemical potential μ . In addition, recently new lattice data for the pure gluon QCD sector defining the effective Polyakov loop potential have been obtained²¹ which differ noticeably from the old data²².

In this paper we investigate how the input information from lattice QCD and the used forms of the effective potential influence general properties of thermodynamics at finite temperature T and baryon chemical potential μ . After introduction, in Sect. 2 we consider the polynomial and logarithmic parameterizations of the Polyakov loop effective potential for the new and old pure gluon lattice data within the two-flavor PNJL model. Independent of the temperature, the model parameters defined by properties of quarks and mesons are presented in Sect. 3. Comparative study of the thermodynamics and phase structure, their dependence on the lattice input and used parametrization are considered in Sect. 4 at finite T and μ . The last Section summarizes the obtained results.

1.1. The Nambu–Jona-Lasinio model with Polyakov-loop

The deconfinement in the pure $SU(N_c)$ gauge theory can be simulated by introducing an effective potential for a complex Polyakov loop field. The PNJL Lagrangian employed in this work is³

$$\mathcal{L}_{\text{PNJL}} = \bar{q} (i\gamma_\mu D^\mu - \hat{m}_0) q + G \left[(\bar{q}q)^2 + (\bar{q}i\gamma_5 \vec{\tau} q)^2 \right] - \mathcal{U}(\Phi[A], \bar{\Phi}[A]; T) . \quad (1)$$

Here, a local chirally symmetric scalar-pseudoscalar four-point interaction of quark fields q, \bar{q} is introduced with an effective coupling strength G , $\vec{\tau}$ is the vector of Pauli matrices in flavor space, \hat{m}_0 is the diagonal matrix of the 2-flavor current quark masses, $\hat{m}_0 = \text{diag}(m_u^0, m_d^0)$, $m_u^0 = m_d^0 = m_0$.

The quark fields are coupled to the gauge field A^μ through the covariant derivative $D^\mu = \partial^\mu - iA^\mu$. The gauge coupling g is conveniently absorbed in the definition $A^\mu(x) = g\mathcal{A}_a^\mu \frac{\lambda_a}{2}$ where \mathcal{A}_a^μ is the $SU(3)$ gauge field and λ_a is the Gell-Mann ma-

trices. The gauge field is taken in the Polyakov gauge $A^\mu = \delta_0^\mu A^0 = -i\delta_4^\mu A_4$. The field Φ is determined by the trace of the Polyakov loop $L(\vec{x})$ and its conjugate³

$$\Phi[A] = \frac{1}{N_c} \text{Tr}_c L(\vec{x}) , \quad \bar{\Phi}[A] = \frac{1}{N_c} \text{Tr}_c L^\dagger(\vec{x}) ,$$

where $L(\vec{x}) = \mathcal{P} \exp \left[i \int_0^\beta d\tau A_4(\vec{x}, \tau) \right]$, $\beta = 1/T$ being the inverse temperature. In the absence of quarks, we have $\Phi = \bar{\Phi}$ and the Polyakov loop serves as an order parameter for deconfinement.

The gauge sector of the Lagrangian density (1) is described by an effective potential $\mathcal{U}(\Phi[A], \bar{\Phi}[A]; T)$. The effective potential must satisfy the $Z(3)$ center symmetry. In accordance with the underlying $Z(3)$ symmetry, one can choose the following general polynomial form:

$$\frac{\mathcal{U}(\Phi, \bar{\Phi}; T)}{T^4} = -\frac{b_2(T)}{2} \bar{\Phi}\Phi - \frac{b_3}{6} (\Phi^3 + \bar{\Phi}^3) + \frac{b_4}{4} (\bar{\Phi}\Phi)^2 , \quad (2)$$

$$b_2(T) = a_0 + a_1 \left(\frac{T_0}{T} \right) + a_2 \left(\frac{T_0}{T} \right)^2 + a_3 \left(\frac{T_0}{T} \right)^3 . \quad (3)$$

The $Z(3)$ symmetry leads to some freedom in the choice of the effective potential form. Along with the simplest polynomial form, Eq.(2), there exists an expression with a logarithm in place of the higher order polynomial terms in $\bar{\Phi}, \Phi$ ². In the logarithmic form the potential is

$$\frac{\mathcal{U}(\Phi, \bar{\Phi}; T)}{T^4} = -\frac{1}{2} a(T) \bar{\Phi}\Phi + b(T) \ln [1 - 6\bar{\Phi}\Phi + 4(\bar{\Phi}^3 + \Phi^3) - 3(\bar{\Phi}\Phi)^2] , \quad (4)$$

$$a(T) = \tilde{a}_0 + \tilde{a}_1 \left(\frac{T_0}{T} \right) + \tilde{a}_2 \left(\frac{T_0}{T} \right)^2 , b(T) = \tilde{b}_3 \left(\frac{T_0}{T} \right)^3 . \quad (5)$$

The pressure of a pure-gauge system is given by $p = -\mathcal{U}$.

Pure-gluon lattice data from Ref. ²² are traditionally used to find the parameter set for both forms of the effective potential^{3,23}. In contrast, our work is based on new gluon lattice data²¹ looking for a new potential to fit the lattice pressure. In finding the potential parameters the following conditions should be satisfied: $\Phi \rightarrow 1$ and $p/T^4 \rightarrow 1.75$, when $T \rightarrow \infty$. As immediately follows from these conditions, $\tilde{a}_0 = 3.51$ for the logarithmic potential and the constraint $1.75 = a_0/2 + b_3/3 - b_4/4$ for the polynomial potential. Minimizing $\mathcal{U}(\Phi, \bar{\Phi}, T)$ with respect to variation of Φ and taking into account that $\Phi = \bar{\Phi}$ at $\mu = 0$, we can find parameters using the method of least mean squared deviations. Thus, for the critical temperature $T_0 = 270$ MeV the following parameter sets were obtained (see Table 1 and Table 2).

In Fig. 1, old and new lattice gluon data are compared together with the results of their approximations. As is seen the lattice results differ by about 10% at $T/T_0 \gtrsim 2$. New data are plotted by circles but the density of measured points is so high that

the results look like a shaded band. Both polynomial and logarithmic forms are in nice agreement with the data and it is hard to distinguish them from each other.

In general, the parameter T_0 depends on the number of active flavors and the chemical potential⁸. In the pure gauge sector $T_0 = 0.27$ GeV was used²¹. The effective potential for both sets of parameters at $T = 0.2, 0.27, 0.32, 0.54$ GeV is shown in Fig. 2. Both sets describe quite satisfactorily the Polyakov loop as a function of

Table 1. Parameters of the effective potential $\mathcal{U}[A]$ with the polynomial form.

	a_0	a_1	a_2	a_3	b_3	b_4
old data ²²	6.75	-1.95	2.625	-7.44	0.75	7.5
new data ²¹	6.47	-4.62	7.95	-9.09	1.03	7.32

Table 2. Parameters of the effective potential $\mathcal{U}(\Phi, \bar{\Phi}; T)$ in the logarithmic form.

	\tilde{a}_0	\tilde{a}_1	\tilde{a}_2	\tilde{b}_3
old data ²²	3.51	-2.47	15.2	-1.75
new data ²¹	3.51	-5.121	20.99	-2.09

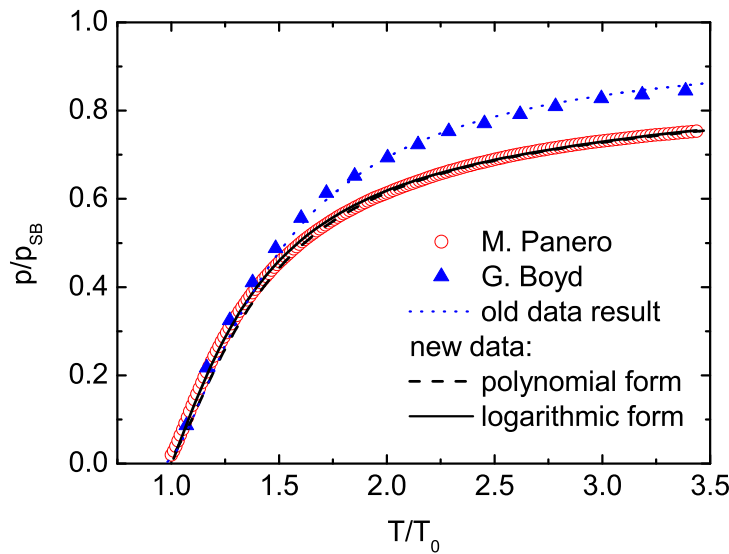


Fig. 1. Scaled pressure in the pure gauge sector as function of scaled temperature. The old²² and new²¹ lattice data are plotted by circles and triangles, respectively. Solid lines correspond to polynomial form of potential and dashed lines correspond to the logarithm form.

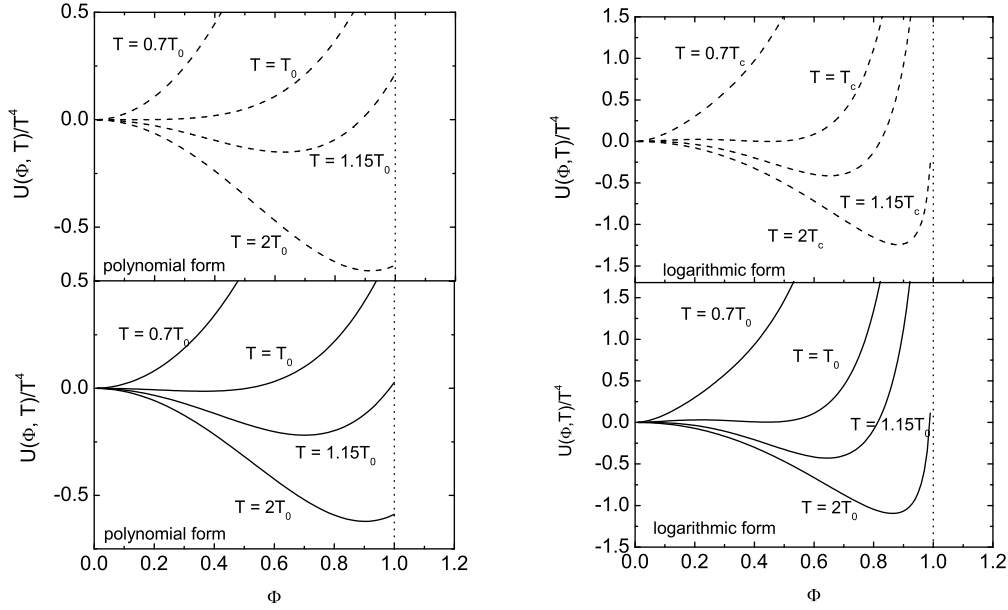


Fig. 2. The Polyakov loop effective potential \mathcal{U} as a function of Φ for various values of temperature for old (top) and new (bottom) sets of parameters. Left panel corresponds to the polynomial form and right panel corresponds to the logarithm form of the potential.

temperature. In accordance with the $Z(3)$ center symmetry, the following properties of the effective potential $\mathcal{U}(\Phi, \bar{\Phi}; T)$ are seen. At low temperature $\mathcal{U}(\Phi, \bar{\Phi}; T)$ has a single minimum at $\Phi = 0$ (a confinement phase); the effective potential is getting flat for the critical temperature $T = T_0$ and above critical temperature (a deconfinement phase) a second minimum arises at nonzero Φ , as a consequence of $Z(3)$ symmetry breaking; in the $T \rightarrow \infty$ limit, $\Phi \rightarrow 1$ (see Fig. 2). One should note that after the second minimum the logarithmic potential Φ increases faster than the polynomial one forming a more distinct minimum. With the introduction of quarks the critical temperature goes down. The range of applicability of this model is $T \lesssim 2.5T_c$ since at higher temperature transverse gluons start to contribute significantly²⁴.

The Polyakov loop is compared with the lattice results in Fig. 3. In reasonable agreement of both forms with the lattice data, the new parameter set predicts slightly lower values of the field Φ because the pressure for new data is also below the old one.

2. Quarks and light mesons in the PNJL model

The grand potential density for the PNJL ($N_f = 2$) model in the mean-field approximation is given by the following equation^{3,9}:

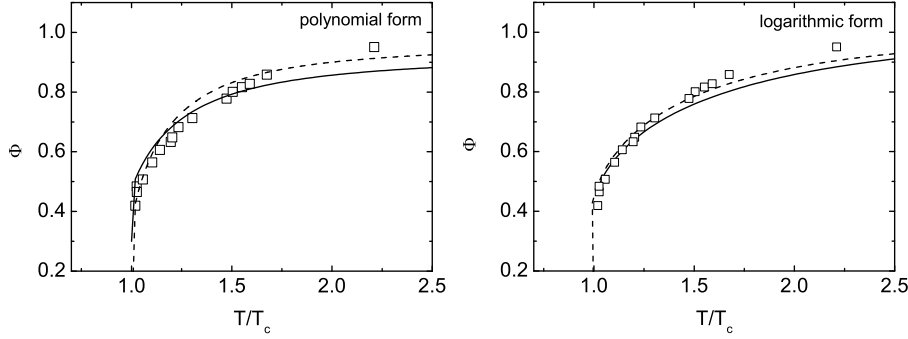


Fig. 3. Temperature dependence of the Polyakov loop Φ for polynomial (2) (left) and logarithmic (4) (right) forms. Lattice data are from ²⁵ Solid and dashed lines correspond to new and old parameter sets, respectively.

$$\Omega(\Phi, \bar{\Phi}, m, T, \mu) = \mathcal{U}(\Phi, \bar{\Phi}; T) + G \langle \bar{q}q \rangle^2 + \Omega_q, \quad (6)$$

where the quark term is

$$\Omega_q = -2N_c N_f \int \frac{d^3p}{(2\pi)^3} E_p - 2N_f T \int \frac{d^3p}{(2\pi)^3} [\ln N_{\Phi}^+(E_p) + \ln N_{\Phi}^-(E_p)] \quad (7)$$

and the functions are

$$N_{\Phi}^+(E_p) = \left[1 + 3 \left(\Phi + \bar{\Phi} e^{-\beta E_p^+} \right) e^{-\beta E_p^+} + e^{-3\beta E_p^+} \right], \quad (8)$$

$$N_{\Phi}^-(E_p) = \left[1 + 3 \left(\bar{\Phi} + \Phi e^{-\beta E_p^-} \right) e^{-\beta E_p^-} + e^{-3\beta E_p^-} \right], \quad (9)$$

where $E_p = \sqrt{\mathbf{p}^2 + m^2}$ is the quasiparticle energy of the quark; $E_p^{\pm} = E_p \mp \mu$, the upper sign applying for fermions and the lower sign for antiparticles.

Since NJL-type models are nonrenormalizable, it is necessary to introduce a regularization, e.g., by a cutoff Λ in the momentum integration. Following ⁹, we use in this study the three-dimensional momentum cutoff Λ for vacuum terms and extend this integration to infinity for the matter contributions given by the second term of Eq. 7. A comprehensive study of the differences between the two regularization procedures (with and without cutoff on the quark momentum states at finite temperature) was performed in ¹⁴.

In the mean-field approximation, we can obtain the constituent quark mass m from the condition that the thermodynamic potential (6) will have a minimum with respect to variation of this parameter, $\partial\Omega/\partial m = 0$. This condition is equivalent to the gap equation ^{9,26}

$$m = m_0 - 2G \langle \bar{q}q \rangle, \quad (10)$$

where the quark condensate is defined as $\langle \bar{q}q \rangle = \partial\Omega/\partial m_0$. For the mass gap equation we get

$$m = m_0 + 4GN_c N_f \int_{\Lambda} \frac{d^3p}{(2\pi)^3} \frac{m}{E_p} [1 - f^+ - f^-] \quad (11)$$

with the modified Fermi-Dirac distribution functions for fermions and antifermions

$$f^+ = \left[\left(\Phi + 2\bar{\Phi} e^{-\beta E_p^+} \right) e^{-\beta E_p^+} + e^{-3\beta E_p^+} \right] / N_{\Phi}^+(E_p), \quad (12)$$

$$f^- = \left[\left(\bar{\Phi} + 2\Phi e^{-\beta E_p^-} \right) e^{-\beta E_p^-} + e^{-3\beta E_p^-} \right] / N_{\bar{\Phi}}^-(E_p). \quad (13)$$

Moreover, for PNJL calculations we should find the values of Φ and $\bar{\Phi}$ by minimizing Ω with respect to Φ and $\bar{\Phi}$ ⁹ at given T and μ . One should note that if $\Phi \rightarrow 1$, the expressions Eqs. (12),(13) reduce to the standard NJL model.

For a self-consistent description of the particle spectrum in the mean-field approximation, the meson correlations have to be taken into consideration. These correlations are related to the polarization operator of constituent fields. For scalar and pseudoscalar particles the polarization operators are represented by loop integrals^{10,11,27}

$$\Pi_{ab}^{PP}(P^2) = \int \frac{d^4p}{(2\pi)^4} \text{Tr} [i\gamma_5 \tau^a S(p+P) i\gamma_5 \tau^b S(p)], \quad (14)$$

$$\Pi_{ab}^{SS}(P^2) = \int \frac{d^4p}{(2\pi)^4} \text{Tr} [S(p+P)S(p)], \quad (15)$$

where $S(p)$ is the quark propagator and the operation Tr is taken over Dirac, flavor and color indices of quark fields.

From the point of view of the polarization operators, the pseudoscalar (π) and scalar (σ) meson masses can be defined by the condition that for $P^2 = M_{\pi}^2$ (M_{σ}^2) the corresponding polarization operator $\Pi^{PP}(M_{\pi}^2)$ ($\Pi^{SS}(M_{\sigma}^2)$) leads to a bound state pole in the corresponding meson correlation function⁹. For mesons at rest ($\mathbf{P} = 0$) in the medium, these conditions correspond to the equations

$$1 + 16GN_c N_f \int \frac{d^3p}{(2\pi)^3} \frac{E_p}{M_{\pi}^2 - 4E_p^2} (1 - f^+ - f^-) = 0, \quad (16)$$

$$1 + 16GN_c N_f \int \frac{d^3p}{(2\pi)^3} \frac{1}{E_p} \frac{E_p^2 - m^2}{M_{\sigma}^2 - 4E_p^2} (1 - f^+ - f^-) = 0. \quad (17)$$

In order to solve Eqs. (10), (16) and (17), a set of model parameters has to be determined: the above-mentioned cutoff parameter Λ , the current quark mass m_0 (in the chiral limit $m_0 = 0$) and the coupling constant G . These parameters are fixed at $T = 0$ to reproduce physical quantities: the pion mass $M_{\pi} = 0.139$ GeV, the pion decay constant $F_{\pi} = 0.092$ GeV and the quark condensate $\langle \bar{q}q \rangle^{1/3} = -250$ MeV. The obtained parameters are the same as in those obtained earlier in our papers^{28,29} and are shown in Table 3. Meson masses obtained as solutions of the

Table 3. The set of model parameters reproducing observable quantities (in brackets) and the chiral condensate $\langle \bar{q}q \rangle^{1/3} = -250$ MeV.

m_0 [MeV]	Λ [GeV]	G [GeV] $^{-2}$	F_π [GeV]	M_π [GeV]
5.5	0.639	5.227	(0.092)	(0.139)

gap-equation (10) and Eqs. (16), (17) at nonzero T are presented in Fig. 4 for two parameter sets.

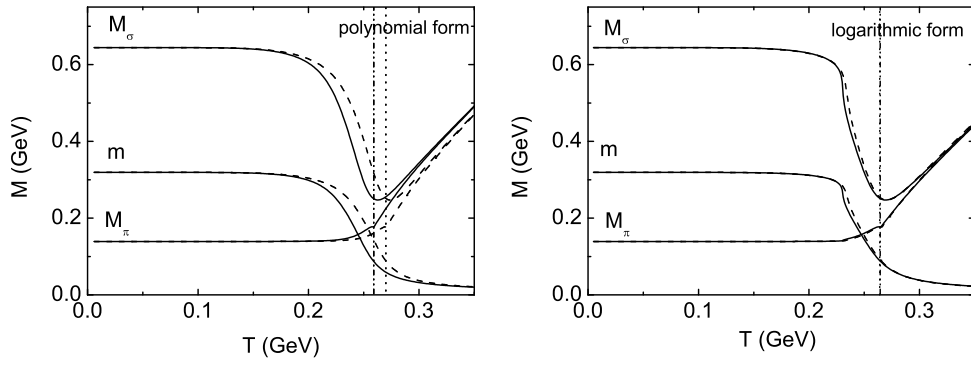


Fig. 4. Temperature dependence of the masses m_q , M_π and M_σ masses at $\mu = 0$ GeV for polynomial (left panel) and logarithmic (right panel) forms of potential. The PNJL results for new and old parameter sets are given by the solid and dashed lines, respectively. The Mott temperatures for both parameter sets are plotted by vertical lines.

The temperature modification of the quasiparticle properties is clearly seen in this figure. Up to the Mott temperature T_{Mott} , defined as $M_\pi(T_{\text{Mott}}) = 2m_q(T_{\text{Mott}})$, the σ mass practically follows the behavior of $2m_q(T)$ with a drop toward the pion mass signaling partial chiral symmetry restoration. At $T > T_{\text{Mott}}$ the masses of chiral partners become equal to each other, $M_\sigma \approx M_\pi$, and then both masses monotonically increase with temperature. Below the Mott temperature, the pion mass remains practically constant. It justifies that T_{Mott} is a little bit lower for the new parameterization than for the old one when the polynomial form is used, while both values of T_{Mott} coincide in the case of logarithmic parametrization.

3. Thermodynamics of the PNJL models

The thermodynamics of particles is described in terms of the grand canonical ensemble which is related to the Hamiltonian H as follows:

$$e^{-\beta V \Omega} = \text{Tr } e^{-\beta(H - \mu N)}, \quad (18)$$

where N is the particle number operator, μ is the quark chemical potential and the operator Tr is taken over momenta as well as color, flavor and Dirac indices. If Ω is known, the basic thermodynamic quantities - the pressure p , the energy density ε , the entropy density s , the density of quark number n and the specific heat c_v - can be defined as follows:

$$p = -\frac{\Omega}{V}, \quad (19)$$

$$s = -\left(\frac{\partial \Omega}{\partial T}\right)_\mu, \quad (20)$$

$$\varepsilon = -p + Ts + \mu n, \quad (21)$$

$$n = -\left(\frac{\partial \Omega}{\partial \mu}\right)_T, \quad (22)$$

$$c_v = \frac{T}{V} \left(\frac{\partial s}{\partial T}\right)_\mu. \quad (23)$$

The thermodynamic potential in equilibrium corresponds to a global minimum

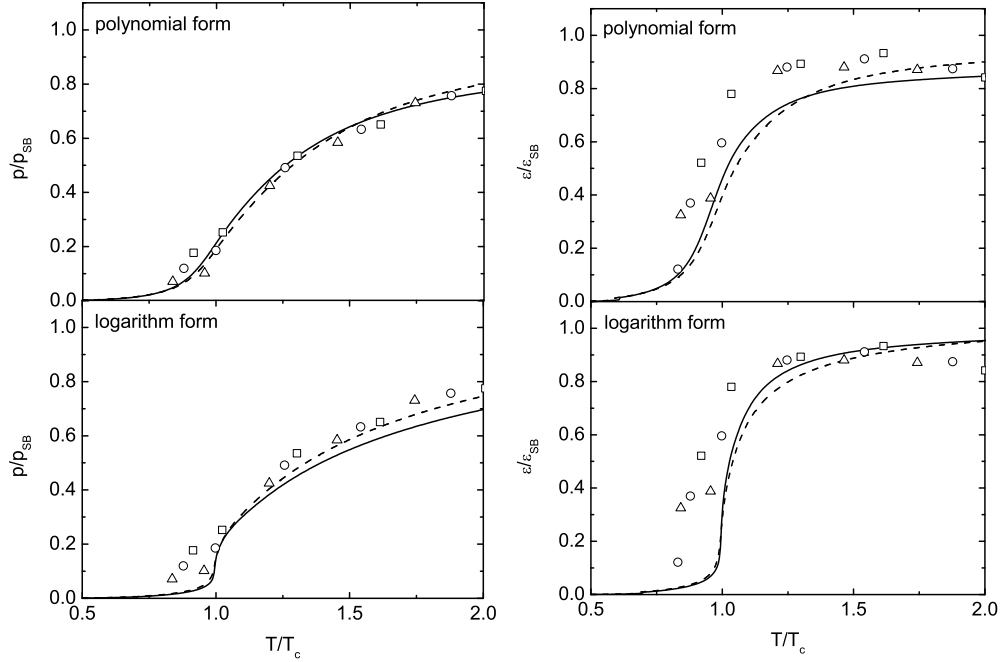


Fig. 5. The temperature dependence of the scaled pressure and energy density within the PNJL model for $\mu = 0$ in two schemes of parametrization. Dotted lines correspond to the old data parameterization and solid lines are new ones. Lattice data points for $N_f = 2$ at $\mu = 0$ are from Ref. 30. Circles, squares and diamonds correspond to calculations at $N_t = 6$ with the mass ratio of the pseudoscalar to vector meson $m_{PS}/m_V = 0.65, 0.70$ and 0.75 , respectively.

with respect to variations of the order parameter

$$\frac{\partial \Omega(T, \mu, m)}{\partial m} = 0, \quad \frac{\partial^2 \Omega(T, \mu, m)}{\partial m^2} \geq 0. \quad (24)$$

All these relations (19),(20),(21),(22),(23) describe the thermodynamics of the system. For the considered models the thermodynamic potentials are defined from Eq. (6). From this equation we can read off the vacuum part

$$\Omega_{vac} = \frac{(m - m_0)^2}{4G} - 2N_c N_f \int \frac{d^3 p}{(2\pi)^3} E_p. \quad (25)$$

This quantity does not vanish as $T \rightarrow 0$ and $\mu \rightarrow 0$. Therefore, in order to obtain the physical thermodynamical potential which corresponds to vanishing pressure and energy density at $(T, \mu) = (0, 0)$, one has to renormalize the thermodynamic potential by subtracting its vacuum expression (25). This corresponds to the following definition of the physical pressure

$$\frac{p}{T^4} = \frac{p(T, \mu, m) - p(0, 0, m)}{T^4}. \quad (26)$$

With increasing temperature the pressure has to reach the Stefan-Boltzmann limit ¹⁴ which in the chiral limit for the PNJL model is given as

$$\frac{p_{SB}}{T^4} = (N_c^2 - 1) \frac{\pi^2}{45} + N_c N_f \frac{7\pi^2}{180} \simeq 4.053, \quad (27)$$

where the first and second terms correspond to gluons and quarks, respectively.

If the regularization $\Lambda = 0.639$ is used, the T -behaviour of the thermodynamic quantities considered is roughly the same while their absolute values are noticeably lower, being far from the Stefan-Boltzmann limit ¹⁴.

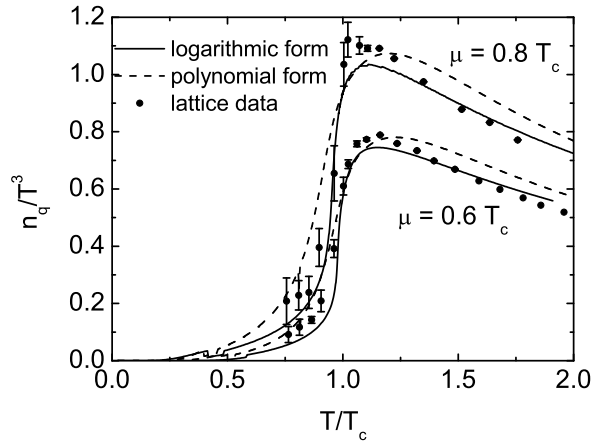


Fig. 6. Comparison of the scaled quark number density as a function of temperature at $\mu = 0.8$ and 0.6 GeV. Lattice data points are from Ref. 31.

Within the PNJL model with $\Lambda \rightarrow \infty$ (we can use $\Lambda \rightarrow \infty$ because most of the integrals in the PNJL are convergent) the reduced pressure and energy density exhibit reasonable behavior consistent with the recent lattice QCD results for the vanishing chemical potential³⁰ (see Fig. 5) keeping in mind that the m_{PS}/m_V ratio in lattice calculations is still far from that for physical masses $m_{PS}/m_V \sim 0.2$. As another example of thermodynamic characteristics, the temperature dependence of the reduced quark number density n_q/T^3 (see Eq.(22)) is presented in Fig. 6. Model results are in good agreement with the lattice data for both values of the chemical potential considered. The logarithmic approximation of the effective potential \mathcal{U} seems to describe lattice data better than the polynomial one.

3.1. Phase diagram and the CEP

Within NJL-like models there are several characteristic temperatures. The parameter T_0 entering into the effective potential (3) of the PNJL model has been noted above. For π -mesons, the Mott temperature T_{Mott} is provided by the condition $M_\pi(T_{\text{Mott}}) = 2m_q(T_{\text{Mott}})$. Above T_{Mott} the pion dissociates into a quark and antiquark and does not exist as a bound state. Similarly the σ meson dissociation temperature T_d^σ is given by the equation $M_\sigma(T_d^\sigma) = 2M_\pi(T_d^\sigma)$ ^{11,13}. Other characteristics of phase transitions are the pseudo-critical temperature for the chiral crossover T_χ , defined by the maximum of $\partial\langle\bar{q}q\rangle/\partial T$, and the pseudo-critical temperature for the crossover deconfinement transition T_p that can be found from the maximum of $\partial\Phi/\partial T$. Their difference is less than 0.013 but it increases with decreasing T_0 . The third quantity is T_c assumed to equal T_χ . But in the PNJL model it is higher than the lattice result $T_c \sim 192$ GeV. Thus, it was suggested to define T_c as an average of two transition temperatures T_χ and T_p ^{3,7}.

All these quantities obtained at $\mu = 0$ are presented in Table 4.

Table 4. Characteristic temperatures in the PNJL models for $\mu=0$.

		T_χ	T_p	T_c	T_{Mott}	T_d^σ
Polynomial form of potential	new	0.2455	0.2335	0.2395	0.259	0.247
	old	0.2575	0.2485	0.253	0.27	0.257
Logarithmic form of potential	new	0.2305	0.2295	0.23	0.264	0.2645
	old	0.2345	0.2335	0.234	0.2645	0.252

To define the crossover transition line, the chiral condensate $\langle\bar{q}q\rangle$ and the Polyakov loop Φ were used as the order parameters. As shown in Fig. 7, these quantities are the temperature-dependent functions and demonstrate a quick change near the transition line which essentially depends on the chemical potential μ . The position of this line is defined by local maximum of $d\langle\bar{q}q\rangle/dT=0$ and $d\Phi/dT=0$. To find the first order transition line, it is convenient to introduce the baryon number susceptibility $\chi_q = \frac{dn_q}{d\mu}|_{T=\text{const}}$. The first order phase transition ends just at point

where χ_q has a pronounced maximum and this point is called critical endpoint (CEP) where the phase transition of the second order. At $T \geq T_{\text{CEP}}$ the baryon number susceptibility has a sharp rise and it can be considered as the presence of an ideal gas of weakly interacting quarks.

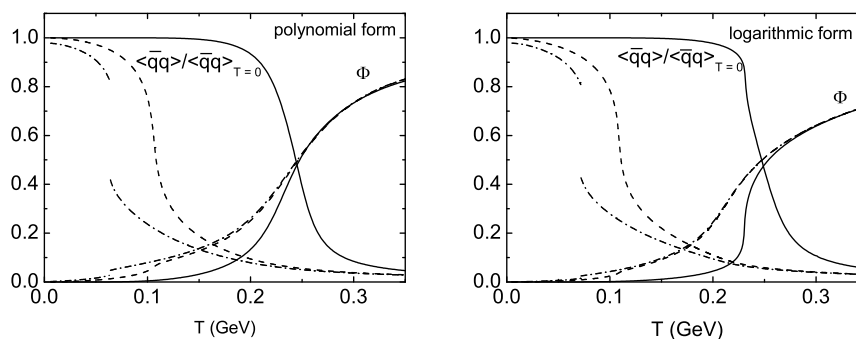


Fig. 7. Temperature dependence of the chiral condensate and Polyakov loop potential with the new set of parameters within the PNJL model. Solid, dashed and dot-dashed lines are calculated for $\mu = 0$, $\mu = \mu_{\text{CEP}}$ and $\mu > \mu_{\text{CEP}}$, respectively.

The behavior of the baryon number susceptibility χ_q as a function of the chemical potential for three different temperatures around the CEP is presented in Fig. 8. For $T < T_{\text{CEP}}$, $\mu > \mu_{\text{CEP}}$ we have a phase transition of the first order with clear discontinuity; for $T = T_{\text{CEP}}$ the susceptibility χ_q diverges at $\mu = \mu_{\text{CEP}}$; for $T > T_{\text{CEP}}$ the discontinuity at the transition line disappears and we observe crossover type of the phase transition. The polynomial and logarithmic approximations of the Polyakov loop predict very similar results. Similar behavior exhibits also the specific heat c_v .

As is seen from Fig. 8, both models show the CEP at the temperature $T_{\text{CEP}} = T_\chi$ below which the chiral phase transition is of the first order. At this point $(T_{\text{CEP}}, \mu_{\text{CEP}})$ the phase transition changes from the first order to crossover^{14,15,16}. At this point the second order transition is present.

The phase diagram in the (T, μ) plane is presented in Fig. 9. Within the PNJL model the positions of the critical endpoints $(T_{\text{CEP}}, \mu_{\text{CEP}})$ are $(0.118, 0.3166)$, $(0.11, 0.3192)$ for the logarithmic form and $(0.10, 0.3175)$, $(0.09, 0.322)$ for the polynomial form, where the first pair of numbers correspond to the new data set and the second one is for the old data set (in GeV). As was noted in Ref.¹⁴, critical properties of observables are significantly influenced by the chosen parameter set and regularization procedure. As follows from Fig. 9, the substitution of the new basic lattice data with using the polynomial and the logarithmic forms for the \mathcal{U} approximation influences more significantly the chemical potential of the critical endpoint μ_{CEP} rather than its temperature T_{CEP} .

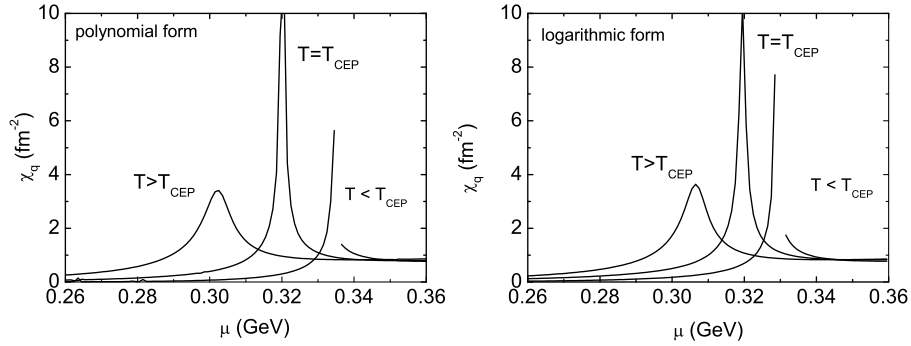


Fig. 8. Baryon number susceptibility around the critical endpoint as a function of the chemical potential for polynomial (left panel) and logarithmic (right panel) form of potential.

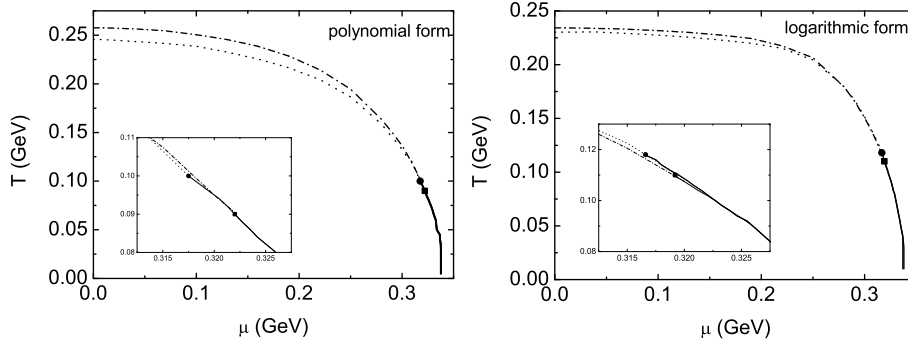


Fig. 9. Phase diagrams of the PNJL model with polynomial (left panel) and logarithmic (right panel) forms of the potential. Solid lines correspond to the first order phase transition, dotted and dot-dashed lines are crossover for new and old lattice data, respectively. The phase region near the critical endpoints is zoomed in the insert.

4. Summary and conclusions

We have considered the PNJL ($N_c = 3, N_f = 2$) model and investigated its phase structure at finite T and μ . Two different sets of parameters based on the old and new lattice data for the pure gluon sector were used and for each of these sets the two different parameterizations of the effective potential $\mathcal{U}(\Phi, \bar{\Phi}, T)$ - polynomial and logarithmic - were applied. The thermodynamics for all the developed versions of the PNJL model was studied and compared with the available lattice data. Consideration of different thermodynamic observables like pressure and energy density, their T and μ behavior as well as the quark number density serves as an important probe of the model. We found that in spite of a noticeable disagreement between the old and new original lattice data, the effective gluon potentials \mathcal{U} are quite close to each other and a larger difference is due to the form of their approximation: the

logarithmic form predicts a more distinct and narrower minimum at high T .

The model qualitatively reproduces both π and σ meson properties in hot, dense quark matter and the rich and complicated phase structure of this medium providing information on the order of phase transitions and the position of critical points. This information depends stronger on the form of the effective potential rather than on the used lattice data set.

Unfortunately, the position of the calculated CEP in the (T, μ) plane is still far from the predictions of lattice QCD and empirical analysis. Further elaboration of the presented model is needed. In particular, the inclusion of entanglement interactions between quark and gauge degrees of freedom in addition to the covariant derivative in the original PNJL model³² and the incorporation of explicit diquark degrees of freedom³³ are of great interest. Both modifications^{32,33} reproduce lattice data at $\mu \geq 0$ better than the original PNJL model and influence the position and the nature of the critical endpoint in the (T, μ) phase diagram. Moreover, with the use of the logarithmic form of the effective potential, these models result in the appearance of new phases.

One should note that we are restricted to the case without diquark correlations and thus possible color superconducting phases at low T and high μ are ignored. It is attractive also to include into consideration the color superconducting phases and nonlocality of the interaction³⁴ as well as effects beyond the meanfield^{18,35}.

Acknowledgments

We are grateful to D. Blaschke and P. Costa for useful comments and constructive suggestions. V.T. acknowledges financial support from the Helmholtz International Center (HIC) for FAIR within the LOEWE program. The work of Yu. K. was supported by RFBR grant No. 09-01-00770a.

References

1. P. N. Meisinger, T. R. Miller, and M. C. Ogilvie, Phys. Rev. **D 65**, 034009 (2002).
2. K. Fukushima, Phys. Lett. **B591**, 277 (2004).
3. C. Ratti, M. A. Thaler and W. Weise, Phys. Rev. **D73**, 014019 (2006).
4. P. Costa, M. C. Ruvio, C. A. de Sousa, and Y. L. Kalinowski, Phys. Rev. **C70**, 025204 (2004).
5. E. Megias, E. Ruiz Arriola and L. L. Salcedo, Phys. Rev. **D74**, 065005 (2006).
6. S. K. Ghosh, T. K. Mukherjee, M. G. Mustafa and R. Ray, Phys. Rev. **D73**, 114007 (2006).
7. S. Rössner, C. Ratti and W. Weise, Phys. Rev. **D75**, 034007 (2007).
8. B. J. Schaefer, J. M. Pawłowski and J. Wambach, Phys. Rev. **D76**, 074023 (2007).
9. H. Hansen, W. M. Alberico, A. Beraudo, A. Molinari, M. Nardi and C. Ratti, Phys. Rev. **D75**, 065004 (2007).
10. H. J. Schulze, J. Phys. **G21**, 185 (1995).
11. E. Quack, P. Zhuang, Y. Kalinovsky, S. P. Klevansky and J. Hüfner, Phys. Lett. **B348**, 1 (1995).
12. D. Horvatic, D. Blaschke, D. Klabucar and O. Kaczmarek, Phys. Rev. **D84** 016005 (2011).

13. W. J. Fu and Y. X. Liu, Phys. Rev. **D 79**, 074011 (2009).
14. P. Costa, M. C. Ruivo, H. Hansen and C. A. de Sousa, Phys. Rev. **D 81**, 016007 (2010).
15. K. Kashiwa, H. Kuono, M. Matsuzaki and M. Yahiro, Phys. Lett. **B 662**, 26 (2008).
16. K. Fukushima, Phys. Rev. **D 78**, 114019 (2008).
17. C. Sasaki, B. Friman and K. Redlich, Phys. Rev. **D 75**, 054026 (2007).
18. D. Blaschke, M. Buballa, A. E. Radzhabov, M. K. Volkov, Yad. Fiz. **71**, 2012-2018 (2008).
19. Z. Zhang and Y. X. Liu, Phys. Rev. **C75**, 064910 (2007).
20. M. Buballa, Phys. Rep. **407**, 205, (2005).
21. M. Panero, Phys. Rev. Lett **103**, 232001 (2009)
22. G. Boyd *et. al*, Nucl. Phys. **B 469**, 419 (1996)
23. S. Rössner, C. Ratti and W. Weise, Phys. Rev. **D75**, 034007 (2007).
24. P. N. Meissner, M. C. Ogilvie and T. R. Miller, Phys. Lett. **B585**, 149 (2004).
25. F. Karsch, E. Laermann and A. Peikert. Nucl. Phys. **B 605**, 579 (2002).
26. J. Hüfner, S. P. Klevansky and P. Zhuang, Acta Phys. Pol. **B 25**, 85 (1994).
27. S. P. Klevansky, Rev. Mod. Phys. **64**, 649 (1992).
28. A. V. Friesen, Yu. L. Kalinovsky and V. D. Toneev, arXiv:1102.1813.
29. A. V. Friesen, Yu. L. Kalinovsky and V. D. Toneev, arXiv:1104.2698.
30. A. Ali Khan *et al.*, Phys. Rev. **D64**, 074510 (2001).
31. C. R. Allton, S. Ejiri, S. J. Hands, O. Kaczmarek, F. Karsch, E. Laermann, and C. Schmidt, Phys. Rev. **D68**, 014507 (2003).
32. Yuji Sakai, Takahiro Sasaki, Hiroaki Kouno, Masanobu Yahiro, arXiv:1104.2394.
33. S. Rössner, C. Ratti and W. Weise, Phys. Rev. **D75**, 034007 (2007).
34. D. Gomez Dumm, D. B. Blaschke, A. G. Grunfeld, N. N. Scoccola, Phys. Rev. **D73**, 114019 (2006).
35. A.E. Radzhabov, D. Blaschke, M. Buballa, M.K. Volkov Phys. Rev. **D83**, 116004 (2011).